arXiv:1611.08521v1 [physics.plasm-ph] 25 Nov 2016

Random and quasi-coherent aspects in particle motion and their effects on transport and turbulence evolution

M. Vlad, F. Spineanu

National Institute of Laser, Plasma and Radiation Physics
Magurele, Bucharest 077125, Romania

E-mail: madalina.vlad@inflpr.ro

Abstract. The quasi-coherent effects in two-dimensional incompressible turbulence are analyzed starting from the test particle trajectories. They can acquire coherent aspects when the stochastic potential has slow time variation and the motion is not strongly perturbed. The trajectories are, in these conditions, random sequences of large jumps and trapping or eddying events. Trapping determines quasi-coherent trajectory structures, which have a micro-confinement effect that is reflected in the transport coefficients. They determine non-Gaussian statistics and flows associated to an average velocity. Trajectory structures also influence the test modes on turbulent plasmas. Nonlinear damping and generation of zonal flow modes is found in drift turbulence in uniform magnetic field. The coupling of test particle and test mode studies permitted to evaluate the self-consistent evolution of the drift turbulence in an iterated approach. The results show an important nonlinear effect of ion diffusion, which can prevent the transition to the nonlinear regime at small drive of the instability. At larger drive, quasi-coherent trajectory structures appear and they have complex effects on turbulence. Key words: turbulence, test particle statistics, test modes, nonlinear effects

1. Introduction

The direct numerical simulations, which have obtained important results in the last decades, largely dominate the actual research in turbulence. The analytical advance based on first principle description and mathematically justifiable approximations is comparatively very small. One cause, perhaps the principal one, is the stochastic advection process, which appears in all turbulent systems. In realistic descriptions of turbulence the advected field are active in the sense that they influence the velocity fields. But, even the most simplified models that deal with passive fields have not been solved analytically in all cases. The cause is the basic problem of particle trajectories in stochastic velocity fields, which can be rather complex in important special cases. One example is the turbulence in incompressible media that is dominantly two dimensional.

The two-dimensional turbulence has a self-organizing character [1]-[4] that consists of the generation of quasi-coherent structure (vortices), which can increase up to the size of the system in special cases as the decaying turbulence in ideal fluids. The tendency to self-organization is partly maintained is weakly perturbed systems [5]-[7]. This property appear at the basic level of particle (tracer) trajectories. They are random sequences of trapping or eddying events and long jumps. The trapping process [8]-[11] strongly modifies the diffusion coefficients and leads to non-Gaussian distribution of displacements.

Theoretical methods for determining the statistics of the advected particles were developed in the last decades and used for the study of various aspects of the transport. The decorrelation trajectory method (DTM, [12]) and the nested subensemble approach (NSA, [13]) are the first semi-analytical methods that are able to go beyond the quasi-linear regime that corresponds to quasi-Gaussian transport. They were specifically developed for the case of two-dimensional incompressible turbulence that is characterized by trajectory trapping or eddying. The general conclusion of these studies is that the existence of space correlations of the stochastic velocity can generate trajectory trapping or eddying, which leads to nonstandard statistics of trajectories: non-Gaussian distributions, long time Lagrangian correlations (memory), strongly modified transport coefficients and an increased degree of coherence. The trapped trajectories form quasi-coherent structures similar to fluid vortices.

Very recent results [14] have shown that these methods could be the basis for the development of a theoretical approach for the study of test modes in turbulent plasmas. It is similar to the Lagrangian approach initiated by Dupree [15], [16] and developed in the 70‘s. The assumption of random trajectories with Gaussian distribution limited the application of Dupree's method to the quasilinear regime. The DTM and NSA enable the evaluation of the average propagator of the test modes in the nonlinear regime and extend the theoretical procedure to the complex processes that are generated in these conditions. The tendency of drift turbulence evolution beyond the quasilinear regime was obtained.

We present a theoretical approach to the study of turbulence evolution, the iterated self-consistent method (ISC). It is based on the analysis of the test particles and test modes in turbulent plasmas. Both test particle and test mode studies start from given statistical description of the turbulence. However, the coupling of these problems can lead to the evaluation of turbulence evolution and to the understanding of the nonlinear processes that are generated. The ISC is applied here to the drift turbulence in magnetically confined plasmas.

The paper is organized as follows. The physical processes analyzed in this paper and the main ideas that are followed in this study are presented in Section 2. Section 3 contains the test particle studies of transport, the DTM and the NSA. A discussion on the representation of the complex trajectories by these methods is also included. The two modules of the ISC (test particle and test mode studies) for the case of drift turbulence are presented in Section 4. The ISC is discussed in Section 5. Section 6

contains the results on the evolution of drift turbulence and the analysis of the nonlinear processes that appear in different conditions (weak and strong drive of the instability). The conclusions are summarized in Section 7.

2. Random and coherent aspects of the trajectories

Numerical simulations have shown that particle trajectories in two-dimensional incompressible stochastic velocity fields are characterized by a mixture of random and quasi-coherent aspects, which appear as a random sequence of large jumps and trapping or eddying events. They are solutions of the equation

$$\frac{dx_i}{dt} = -\varepsilon_{ij}\partial_j\phi(\mathbf{x}(t),t), \tag{1}$$

where $\mathbf{x}(t)$ is the trajectory in rectangular coordinates $\mathbf{x} = (x_1, x_2)$, $\varepsilon_{12} = 1$, $\varepsilon_{21} = -1$, $\varepsilon_{ii} = 0$, and $\phi(\mathbf{x},t)$ is the potential. This is a Hamiltonian system with the conjugate variables represented by the two components of particle trajectories.

The origin of eddying is the Hamiltonian structure of Eq. (1). The trajectories are periodic and they wind on the contour lines of the potential when it is time independent. This defines the state of permanent trapping. The Lagrangian potential is invariant in these conditions and the transport is subdiffusive because the particles are tied on the fixed contour lines of the potential.

If the motion is weakly perturbed (by time variation of the potential or by other components of the motion that can by introduced in Eq. (1)), the trapping is temporary and alternates with large jumps. The statistical importance of the trapping events depends on the strength of the perturbation that is represented by dimensionless factors, which are usually ratios of characteristic times. Two characteristic times are defined in (1): the correlation time of the potential τ_c that gives the scale of the time variation of $\phi(\mathbf{x},t)$ and the time of flight of the particles $\tau_{fl} = \lambda_c/V$, where λ_c is the space scale of $\phi(\mathbf{x},t)$ and V is the amplitude of the velocity. These parameters appear in the Eulerian correlation of the potential defined in Section 3. The characteristic times define the Kubo number $K = \tau_c/\tau_{fl}$, which is a measure of trapping in time dependent potentials. Namely, the permanent trapping corresponds to $K \to \infty$, temporary trapping exists for $K > 1$, and the statistical relevance of trapping is a decreasing function of K. Any other perturbation of the basic Hamiltonian motion defines a characteristic time τ_d for the decorrelation of the trajectory from the potential, and a dimensionless parameter similar to Kubo number, the decorrelation number $K_d = \tau_d/\tau_{fl}$.

The trapping events appear when the trajectory arrives around the maxima and the minima of the potential. The process is quasi-coherent because it affects all the particles situated in these regions in the same way. The high degree of coherence of the trapped trajectories is evidenced in a study of the statistical properties of the distance δx between neighbour trajectories [13]. The time evolution of $\langle \delta x^2(t) \rangle$ is very slow, which shows that neighbour particles have a coherent motion for a long time compared

to τ_{fl}. They are characterized by a strong clump effect with the increase of $\langle \delta x^2(t) \rangle$ that is slower than the Richardson law. These trajectories form intermittent quasi-coherent structures similar to fluid vortices and represent eddying regions. Their average size and life-time depend on the characteristic of the turbulence.

The trapping events appear around the maxima and the minima of the potential. The other particles (that evolve on contour lines corresponding to small absolute values of the potential) have much larger displacements. The large displacements are caused by the large size of these contour lines and also by the decorrelation, which allows transitions between neighbour potential cells. These large jumps are random. The transport is essentially determined by them, while the trapping events have negligible contributions. Thus, trapping can be associated to a process of micro-confinement. At a given moment, the micro-confinement affects a fraction of the particle, and, in a large time interval, every particle is subjected to micro-confinement events during a fraction of this time. The micro-confinement determines the existence of transport reservoirs in the sense that diffusion can be strongly enhanced when these trapped particles are released by the increase of the perturbation strength.

The quasi-coherent trajectory structures have more complex effects in the presence of an average velocity V_d. The probability of the Lagrangian velocity has to be time invariant, as required by the zero divergence of the velocity field. In particular, the average Lagrangian velocity $V(t)$ has to be equal to the average Eulerian velocity at any time. The trapped particles do not contribute to $V(t)$, which means that the free particles have an average velocity larger than V_d in order to compensate the fraction of trapped particles n_{tr}. This effect leads, in the case of a potential that drifts with the velocity V_d, to flows in both directions: the structures move with the potential with the velocity V_d and the free particles have an average motion in the opposite direction with a velocity V_f such that

$$n_{tr} V_d + n_f V_f = 0. \tag{2}$$

The average velocity also determines the release of a part of the trapped particles and the decrease of the size of the trajectory structures. At large V_d, the structures are completely eliminated at

The aim of the paper is to analyze the effects produced by these complex trajectories on the evolution of drift turbulence and on the associated transport.

We show that the physical picture of the trajectories that mix random and quasi-coherent aspects is well represented in the DTM and NSA. The problem of test particle transport and typical results obtained with these methods are presented in Section 3. The image of the random and quasi-coherent aspects given by the DTM and NSA is emphasized and the effects of the micro-confinement are discussed in this Section.

The drift turbulence is analyzed in relation with the random and quasi-coherent aspects of the trajectories (Sections 4 and 6). This type of turbulence determines special effects on transport coefficients, which are presented in Section 4.2, together with the characteristics of the trajectory structures and their influence on the probability of

displacements. The test modes on turbulent plasma are presented in Section 4.1. It is shown that the trajectory structures can lead to strong nonlinear effects. The self-consistent evolution of the drift turbulence obtained with the ISC is finally analyzed in Section 6.

3. Test particle approach to stochastic transport

The Eulerian and the Lagragian correlations are the main concepts in test particle transport. The two point Eulerian correlation (EC) of the velocity is defined as

$$E_{ij}(\mathbf{x},t) \equiv \langle v_i(\mathbf{x}_1,t_1)\ v_j(\mathbf{x}_2,t_2)\rangle\,, \tag{3}$$

where $\mathbf{x}=\mathbf{x}_2-\mathbf{x}_1$, $t=t_2-t_1$ and $i,j=1,2$ account for the two components of the velocity. The main statistical parameters of the velocity field appear in this function. The amplitudes of velocity fluctuation are $V_i^2=E_{ii}(\mathbf{0},0)$, the correlation lengths λ_i are the characteristic decay lengths of the functions $E_{ii}(\mathbf{x},0)$, and the correlation time is defined by the time decay of $E_{ij}(\mathbf{0},t)$. We consider here homogeneous and stationary velocity fields, which have ECs that depend only on the distance between the two points and on the difference between the two times, as (3).

The EC describes the space structure and the time variation of the stochastic velocity field

The Lagrangian velocity correlation (LVC) is defined as

$$L_{ij}(t) \equiv \langle v_i(\mathbf{x}_1,t_1)\ v_j(\mathbf{x}(t;t_1,\mathbf{x}_1)\rangle\,, \tag{4}$$

where $\mathbf{x}(t;t_1,\mathbf{x}_1)$ is the trajectory in a realization of the stochastic field that starts at $t=t_1$ in the point $\mathbf{x}_1$.

The LVC is thus a time dependent function that describes statistical properties of particle motion in the stochastic velocity field. In most cases the LVC decays to zero since the Lagrangian velocity becomes statistically independent on the initial velocity (it decorrelates). The characteristic time τ_d of the LVC decay is the measure of the memory of the stochastic Lagragian velocity. The decorrelation time τ_d is the correlation time τ_c of the EC if particle motion is determined only by the velocity field, and it can be completely different of τ_c in the presence of additional components of the motion (average velocity, collisional diffusivity, etc.)

Besides this important effect of memory, the LVC determines the main quantities related to test particle transport. As shown by Taylor [17], the mean square displacement (MSD) $\langle x_i^2(t)\rangle$ and its derivative, the running diffusion coefficient $D_i(t)$, are integrals of the LVC

$$\left\langle x_i^2(t)\right\rangle = 2\int_0^t d\tau\ L_{ii}(\tau)\ (t-\tau), \tag{5}$$

$$D_{ii}(t) = \int_0^t d\tau\ L_{ii}(\tau). \tag{6}$$

The asymptotic values of $D_i(t)$

$$D_i = \lim_{t\to\infty} D_{ii}(t) = \int_0^\infty L_{ii}(\tau)d\tau \tag{7}$$

are the diffusion coefficients. The time dependent diffusion coefficients provide the "microscopic" characteristics of the transport process. The diffusion at the transport space-time scales, which are much larger than λ_c and τ_c, is described by the asymptotic values D_i.

The aim of the test particle studies is essentially to determine the LVC as function of the EC.

The decorrelation of the Lagrangian velocity after the memory time τ_c leads to the possibility of decomposing the statistics of the displacements at large time $t >> \tau_c$ in a sequence of independent small scale processes of time τ_c. The probability of the small scale displacements (the micro-probability), $P^{\tau_c}(\mathbf{x}, t)$, determines the elementary step of the transport process as the MSD

$$\Delta_i^2 \equiv \left\langle (x_i(t_1 + \tau_c; t_1, \mathbf{x}_1) - \mathbf{x}_1)^2 \right\rangle = \int d\mathbf{x}\ x_i^2 P^{\tau_c}(\mathbf{x}, \tau_c).$$

The statistics of the displacements at large times $t >> \tau_c$ is Gaussian, with the exception of the processes that have $\Delta \to \infty$ or $\tau_c \to \infty$ (see [18], [9]).

The asymptotic diffusion coefficients are usually approximated by a random walk with the step Δ performed in the time τ_c, that is $D_{rw} \cong \Delta^2/\tau_c$.

It is important to underline that the test particle transport gives results that are in very good agreement to those obtained from turbulent fluxes when the space scale of the turbulence is much smaller than the characteristic lengths of the gradients. This is confirmed by the numerical simulations [19], [20].

Most of the theoretical methods are essentially based on Corrsin hypothesis [21], which assume that the micro-probability $P^{\tau_c}(\mathbf{x}, t)$ is Gaussian and that the displacements are statistically independent on the velocity field. They lead to diffusive transport in the limit of static velocity fields ($\tau_c \to \infty$), and thus they cannot apply to the special case of zero divergence two-dimensional velocity fields. It can be shown that a diffusive transport is obtained even when the second assumption is eliminated, which suggest that the micro-probability is not Gaussian in the presence of trapping. The first theoretical approach that finds subdiffusive transport in this special case ([22], [23]) does not use the Gaussian assumption, but it is based on the percolation theory. It only determines the scaling of the asymptotic diffusion coefficients. The detailed statistical information that is contained in the LVC (4) was first obtained by the decorrelation trajectory method (DTM, [12]). This semi-analytical method was developed and validated by the nested subensemble approach (NSA, [13]).

A short review of the DTM and NSA and a discussion of the image they give on the micro-confinement process is presented below.

3.1. The DTM and NSA

Trajectory trapping or eddying is a consequence of the Lagrangian invariance of the potential. The DTM and the NSA were developed having in mind the necessity of evidencing the statistical consequences of this invariance. We have also imposed the condition of performing only the approximations that do not violate this property.

The main idea is to define subensembles of the realizations of the potential that correspond to the same values of the potential and of its derivatives in the starting point of the trajectories $\mathbf{x} = \mathbf{0}$, $t = 0$. A system of nested subensembles is constructed. All the realization with the potential $\phi(\mathbf{0}, 0) = \phi^0$ are grouped together in a subensemble S_0, then S_0 is subdivided into subensembles S_1 according to the values of the first space derivatives of the potential ϕ_i^0, then each S_1 is again divided into smaller subensembles S_2 using the values of the second derivatives ϕ_{ij}^0, and the procedure can continue. The trajectories in a subensemble S_n are super-determined, in the sense that they have supplementary initial condition (the potential ϕ^0, the initial velocity that is the derivative of the potential $\mathbf{v}(\mathbf{0}, 0) = \mathbf{v}^0 = (-\phi_2^0,\ \phi_1^0)$, and higher order derivatives up to the order n). This leads to a high degree of similarity of the trajectories in a subensemble S_n, that increases with the increase of the nesting order n.

The statistical description of the velocity in a subensemble S_n can be derived from the statistics in the whole set of realization using conditional averages. A Gaussian velocity reduced at the subensemble S_n remains Gaussian, but its average and dispersion are modified. The subensemble average $\mathbf{V}^{S_n}(\mathbf{x}, t) \equiv \langle \mathbf{v}(\mathbf{x}, t) \rangle_{S_n}$ exists even in the case of zero average velocities. It is a function of the EC that also depends (linearly) on the set of parameters of the nested subensembles. The subensemble average velocity $\mathbf{V}^{S_n}(\mathbf{x}, t)$ is a space-time dependent function, which has the value $\mathbf{V}^{S_n}(\mathbf{0}, 0) = \mathbf{v}^0$ (where $\mathbf{v}^0 = (-\phi_2^0,\ \phi_1^0)$), as imposed by the conditions that define S_1 in the nested subensembles. The subensemble dispersion $\left\langle (\delta \mathbf{v}(\mathbf{x}, t))^2 \right\rangle_{S_n}$ (where $\delta \mathbf{v}(\mathbf{x}, t) = \delta \mathbf{v}(\mathbf{x}, t) - \mathbf{V}^{S_n}$) is much smaller that the amplitude of the velocity fluctuations in the whole set of realization $\mathbf{V}^2$. It is zero for $\mathbf{x} = \mathbf{0}$ and $t = 0$ (because imposing a condition on the value of the velocity eliminates any fluctuation), and it reaches the value $\mathbf{V}^2$ at distances larger than the correlation lengths λ_i and/or at times larger than the correlation time τ_c. The small amplitude of the velocity fluctuations in the subensemble S_n provides a second contribution to the increase of the degree of similarity of the set of trajectories that yield from the realizations that are included in S_n.

The subensemble average velocity $\mathbf{V}^{S_n}(\mathbf{x}, t)$ has the same structure as particle velocity. It can be derived from a function $\Phi^{S_n}(\mathbf{x}, t)$, which is the subensemble average potential

$$V_i^{S_n}(\mathbf{x}, t) = -\varepsilon_{ij} \frac{\partial \Phi^{S_n}(\mathbf{x}, t)}{\partial_{x_j}}. \tag{8}$$

The potential $\Phi^{S_n}(\mathbf{x}, t)$ is obtained as the conditional average with the set of conditions that define the nested subensembles. Thus, it is equal to ϕ^0 for $\mathbf{x} = \mathbf{0}$ and $t = 0$ for any value of the nesting order n.

The existence of the subensemble average velocity $\mathbf{V}^{S_n}(\mathbf{x},t)$ determines an average trajectory in S_n that is obtained by performing the subensemble average of the equation of motion

$$\frac{d}{dt}\left\langle \mathbf{x}(t)\right\rangle_{S_n} = \left\langle \mathbf{v}(\mathbf{x}(t),t)\right\rangle_{S_n}. \tag{9}$$

The right hand side of this equation is generally very difficult to be evaluated since it is the average of a stochastic function $\mathbf{v}(\mathbf{x},t)$ of a stochastic variable, the trajectory $\mathbf{x}(t)$ that is determined by $\mathbf{v}(\mathbf{x},t)$. However, the high degree of similarity of the trajectories in the subensemble S_n enables an important simplification that consists in neglecting the fluctuations of the trajectories. The average Lagrangian velocity is thus approximated in S_n by the subensemble Eulerian velocity calculated along the average trajectory

$$\frac{d}{dt}\mathbf{X}^{S_n}(t) = \mathbf{V}^{S_n}(\mathbf{X}^{S_n}(t),t), \tag{10}$$

where $\mathbf{X}^{S_n}(t)$ is the approximate subensemble average trajectory in S_n, $\mathbf{X}^{S_n}(t) \cong \left\langle \mathbf{x}(t)\right\rangle_{S_n}$. It is called the decorrelation trajectory (DT), because it shows the way toward decorrelation in each subensemble. We note that the approximation (10) of Eq. (9) is in agreement with the invariance of the Lagrangian potential. Equation (10) has Hamiltonian structure as the equation of particle motion (1). This leads, in the case of static velocity fields, to the invariance of the Lagrangian potential $\Phi^{S_n}(\mathbf{X}^{S_n}(t))$, which is equal to ϕ^0 for any value of the nesting order n.

The LVC, $D_{ii}(t)$ and other Lagrangian averages are determined by summing the contribution of all subensembles. This leads to integrals over the parameters that define the subensembles.

Thus the NSM is a systematic expansion based on the nested subensembles. It is a semi-analytical method that determines the statistics of the stochastic trajectories in terms of the DTs. These trajectories and the integrals over the subensembles have to be numerically calculated. The calculations are at PC level, with run times that increase as the nesting order increases, starting from few minutes for $n = 2$.

The DTM [12] corresponds to the nesting order $n = 1$. The results obtained using the NSM of order $n = 2$ are presented in [13]. The DTs for the subensembles S_2 are completely different of those of the DTM. However they lead to results for the LVC that are not much different of those obtained with the DTM, which shows that the NSM converges fast. The higher order NSM provides more detailed statistical information at the expense of the increase of the number of the DTs and of the complexity of their equation. The statistics of the distance between neighbor trajectories was determined with the $n = 2$ NSM.

We use here the DTM that is based on the subensembles S_0 and S_1. They are defined by the conditions $\phi(\mathbf{0},0) = \phi^0$ and $\mathbf{v}(\mathbf{0},0) = \mathbf{v}^0$. The subensemble S_1 average potential is

$$\Phi^{S_1}(\mathbf{x},t) = \phi^0\frac{E(\mathbf{x},t)}{E(0)} + v_1^0\frac{\partial_2 E(\mathbf{x},t)}{V_1^2} - v_2^0\frac{\partial_1 E(\mathbf{x},t)}{V_2^2}, \tag{11}$$

where $\partial_i E$ are the space derivatives of the EC. Summing the contributions of all subensembles, the Lagragian velocity correlation and the time dependent diffusion coefficient are evaluated as

$$L_{ij}(t) = \int\int d\phi^0 d\mathbf{v}^0 P(\phi^0) P(\mathbf{v}^0)\ v_i^0\ V_j^S\left[\mathbf{X}^S(t), v_{th}t, t\right], \tag{12}$$

$$D_{ij}(t) = \int\int d\phi^0 d\mathbf{v}^0 P(\phi^0) P(\mathbf{v}^0)\ v_i^0\ X_j^S(t), \tag{13}$$

where $P(\phi^0)$ and $P(\mathbf{v}^0)$ are the Gaussian probabilities for ϕ^0 and $\mathbf{v}^0$ respectively.

An important simplification was recently found [24]. We have shown that the number of parameters of the subensembles can be reduced to only two without significant modifications of the diffusion coefficients. The magnitude u of the normalized velocity $v_i(\mathbf{0}, 0)/V_i$ can be eliminated from the definition of S_1. The integral over u can be performed in the subensemble Eulerian correlation in S_1. This leads to a modified average potential, which depends only on ϕ^0 and θ^0, the orientation of the normalized velocity

$$\Phi^{S_1'}(\mathbf{x}, t) = \phi^0 \frac{E(\mathbf{x}, t)}{E(0)} + \sqrt{\frac{8}{\pi}} \cos(\theta^0) \frac{\partial_2 E(\mathbf{x}, t)}{V_1} - \sqrt{\frac{8}{\pi}} \sin(\theta^0) \frac{\partial_1 E(\mathbf{x}, t)}{V_2}. \tag{14}$$

The parameter θ^0 defines a larger subensemble S_1' that includes the subensembles S_1 with any value of u.

The time dependent diffusion coefficients are obtained in this case from

$$D_{11}(t) = \frac{V_i}{2\pi}\sqrt{\frac{\pi}{2}} \int_{-\infty}^{\infty} d\phi^0 P(\phi^0) \int_0^{2\pi} d\theta^0 \cos(\theta^0) X_1^{S'}(t), \tag{15}$$

$$D_{22}(t) = \frac{V_i}{2\pi}\sqrt{\frac{\pi}{2}} \int_{-\infty}^{\infty} d\phi^0 P(\phi^0) \int_0^{2\pi} d\theta^0 \sin(\theta^0) X_2^{S'}(t) \tag{16}$$

where $\mathbf{X}^{S'}(t)$ is the DT in the subensemble S' that is the solution of

$$\frac{dX_i^{S'}}{dt} = V_i^{S'}(\mathbf{X}^{S'}, t) + \delta_{i2} V_d, \tag{17}$$

where we have introduced an average velocity V_d along $\mathbf{e}_2$ axis.

Thus, the diffusion coefficients are obtained by calculating the double integral in Eq. (15) with the DTs determined for each value of ϕ^0, θ^0 from Eq. (17), where the velocity $V_i^{S'}$ is obtained from the potential (14).

Other Lagrangian quantities are obtained using expression similar to (15), which consists of using the DTs for the evaluation of the average Lagragian quantities in S' and of the summation of the contributions of all subensembles.

This is a very fast version of the DTM because the number of DTs is strongly reduced (from N^3 to N^2, where N is the number of discretization points for each parameter of the subensembles).

3.2. Trapping and micro-confinement description by DTM

The decorrelation trajectories (DTs) are the main concept of this theoretical description of trajectory statistics. They are approximations of the average trajectories in the subensembles, which embed the high degree of similarity of the corresponding sets of stochastic trajectories. The probability of each DT is the probability of the parameters of its nested subensembles, which are initial conditions for the DT. Their average on the whole set of realizations (obtained by integrals similar to (15)) is zero. The DTs are in agreement with the invariance of the Lagrangian potential in the static case. Each DT is a periodic functions in this case, and it is tied to the contour line of the subensemble average potential. The Lagragian potential for the DT is ϕ^0, the same with the Lagrangian potential for any trajectory included in S_0.

The DTs describe the Lagragian effects at the turbulence space-time scale. After times longer than the decorrelation time τ_d or after displacements larger than the correlation lengths λ_i, all DTs saturate. The asymptotic values $X_i^{S'}(t) \to l_i^d$ are functions of the parameters of the corresponding nested subensembles, and they represent the average distances traveled during the decorrelation time by the trajectories in the subensembles. Besides, the DTs provide a detailed description of the decorrelation process, which consists of the path through the correlated zone in each subensemble. In particular, trajectory trapping corresponds to $l_i^d < \lambda_i$ for a statistically relevant number of DTs.

The DTs obtained from Eq. (17) for $V_d = 0$ strongly depend on the correlation time τ_c and on the value of $|\phi^0|$.

For fast decorrelation (small τ_c), the DTs are along the initial velocity and they practically do not depend on the initial potential. This type of DTs are specific to the Gaussian transport. The fast decorrelation determines quasilinear (Gaussian) transport.

In the case of slow decorrelation (large τ_c), the DTs are completely different for small and large values of the initial potential. At large values of $|\phi^0|$, the DTs rotate on closed paths with a velocity that decay to zero at times larger than τ_c. The asymptotic displacements are smaller than the correlation length. The DTs with small $|\phi^0|$ have much larger displacements that are predominantly oriented along the direction of the initial velocity. Thus, the typical structure of the real trajectories (that consists of a random sequence of eddying events and jumps) is represented by the DTs. They actually describe segments of trajectories of time intervals of the order τ_c that are either trapping events or free displacements, depending on the initial potential. More important, the statistical relevance of each type of motion and the influence of the trajectory trapping is determined by the whole set of DTs. The slow decorrelation determines nonlinear (non-Gaussian) transport.

The existence of an average velocity V_d in the equation of motion determines modifications of the DTs in the nonlinear regime. The value of $|\phi^0|$ that gives the limit between free and trapped trajectories increases, which means that the fraction of trapped trajectories decreases. The average velocity also produces a new type of

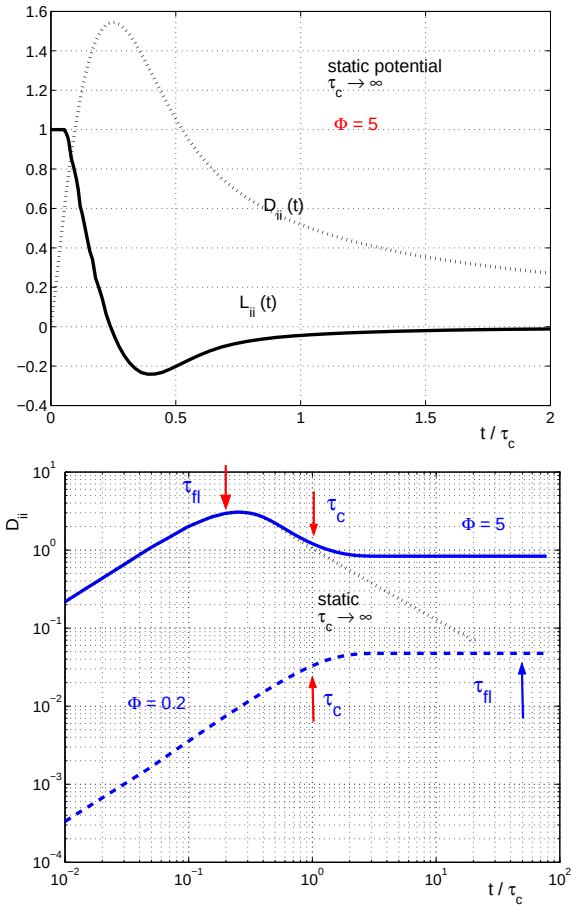

Figure 1. a) The LVC and $D_{ii}(t)$ for the subdiffusive transport ($\tau_c \to \infty$).
b) $D_{ii}(t)$ in the quasilinear (dashed line for $\Phi = 0.2$) and nonlinear (continuous line for $\Phi = 5$) regimes for the correlation time $\tau_c = 1$. The subdiffusive transport is also represented for comparison (dotted line).

DTs. They are opened trajectories that turn toward the direction of $V_d\mathbf{e}_2$.Their number increases as V_d increases and, when V_d is much large than the stochastic velocity, all DTs are of this type. Thus, the average velocity eliminates progressively (as V_d increases) the trapping of the trajectories and eventually leads to quasilinear transport.

Typical results for $D_{ii}(t)$ and for the LVC are shown in Figure 1. They are obtained for isotropic turbulence with the EC of the potential $E = \Phi^2 \exp(-(x_1^2+x_2^2)/\lambda^2/2-t/\tau_c)$ and $V_d = 0$. The diffusion process is isotropic ($D_{11} = D_{22}$) and the decorrelation is produced by the time variation of the potential ($\tau_d = \tau_c$).

Figure 1a presents the case of static potentials ($\tau_c \to \infty$). One can see that the diffusion coefficient has a maximum at a time of the order of the time of flight $\tau_{fl,i} = \lambda_i/V_i$, and then it decays to zero. The DTM yields subdiffusive transport for such fields where the trajectories are tied on the contour lines of the potential. The LVC defined by (4) is negative at large time (Figure 1a), such that its integral decays to zero. It has a negative tail that decays as a negative power of time.

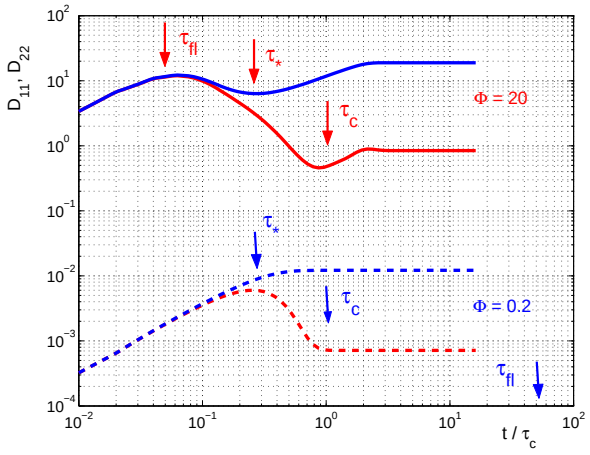

Figure 2. The anisotropic diffusion coefficients in the presence of an average velocity $V_d\mathbf{e}_2$: $D_{11}(t)$ (red) and $D_{22}(t)$ (blue) in the quasilinear regime (dashed lines for $\Phi = 0.2$) and in the nonlinear regime (continuous lines for $\Phi = 20$)

When the potential is not static (τ_c is finite), the transport becomes diffusive. As seen in Figure 1b, $D_{ii}(t)$ has different shapes at small and large amplitudes of the potential fluctuations Φ. The diffusion coefficient increases linearly at small time and it eventually saturates (for $t > \tau_c$) in the case of small Φ (dashed line), while, at large Φ (continuous line), a transitory decay appears before saturation. The decay accounts for the micro-confinement produced by trajectory trapping. This process appears if $\tau_{fl} < \tau_c$ (in general, for $\tau_{fl} < \tau_d$). One can see in Figure 1b that the variation of τ_c determines opposite effects in the two cases. The decrease of τ_c leads to the decrease of the asymptotic diffusion coefficient in the quasilinear case and to the increase of D_i for the nonlinear transport.

The effect of an average velocity V_d is shown in Figure 2. The diffusion becomes non-isotropic, but the differences appear in $D_{ii}(t)$ only for $t > \tau_*$, where τ_* is the characteristic time defined by the average velocity $\tau_* = \lambda/V_d$. In the case of the quasilinear transport (dashed lines for $\Phi = 0.2$), both coefficients decrease, but D_{11} much more. It saturates for $t > \tau_c$, after a significant decrease during the interval (τ_*, τ_c). The diffusion coefficient D_{22} saturates at τ_* and it does not depend on the decorrelation time if $\tau_d > \tau_*$. This shows that the average velocity determines the decorrelation along its direction and has a decaying effect for the diffusion along the density gradient. In the nonlinear regime, the average velocity determines a strong increase of D_{22} and a small decrease of D_{11}, as seen in Figure 2 (the continuous lines).

The LVC for the unperturbed static potential (Figure 1a) is the result of the permanent trapping. It shows that the process has a long memory (the decay at large time of the LVC is of the power law type $L_{ii}(t) \sim t^{-\nu}$, where $\nu > 0$). Its positive and negative parts compensate, such that the time integral, which in the diffusion coefficient $D_{ii}(t)$, decays to zero at large time. This behaviour is the representation of the micro-

confinement.

Any small perturbation (characterized by a large decorrelation time τ_d) has significant effect due to the existence the long time correlation of the Lagrangian velocity. It destroys the equilibrium between the positive and the negative parts of the LVC and leads to finite values of the asymptotic diffusion coefficient. For instance, the time variation of the potential determines the cutting of the LVC at the correlation time τ_c and consequently the saturation of $D_{ii}(t)$, as seen in Figure 1b. This is the representation of the perturbation of the micro-confinement by releasing a part of trajectories. The transport reservoir is the maximum of $D_{ii}(t)$ (Figure 1a). It provides the maximum diffusion coefficient that correspond the a decorrelation process with $\tau_d = \tau_{fl}$, which can release all the trapped trajectories.

Various aspects of the transport in fusion plasmas were studied using the DTM, that was developed and adapted to the study of models with increased complexity [24]-[36].

4. Test modes and test particles in drift turbulence

Drift instabilities are low-frequency modes generated in nonuniform magnetically confined plasmas [37]. We consider here the basic drift instability in uniform magnetic field. It belong to the family of instabilities that have the main role in particle and energy transport in fusion research [2], [38], [39]. They have complex nonlinear evolution with generation of large correlations and zonal flow modes [5]-[7].

Test modes and test particle studies start from the given statistical description of turbulence. They provide answers to different questions compared to the case self-consistent studies. Namely, they evaluate the growth rates of the modes, the diffusion coefficients and the characteristics of the transport as functions of the parameters of the background turbulence. The self-consistent studies determine the characteristics of the turbulence generated in given macroscopic conditions (as density gradient, temperatures) and the associated transport. We show in Section 6 that an iterated self-consistent (ISC) method can be developed for the drift turbulence. It is based on the coupled study of test particle and test modes. These main modules of the ISC theory are presented here.

The DTM and the NSA provide the basis for the development of a Lagrangian method for the study of test modes in turbulent plasmas. It is similar to the approach initiated by Dupree [15], [16]. The assumption of random trajectories with Gaussian distribution limited the application of Dupree's method to the quasilinear regime. The novelty of our approach consists of the statistical description of the trajectories, which includes both random and coherent aspects. The latter lead to non-Gaussian distribution of trajectories and to complex Lagrangian correlations.

This section is a short review of previous work [25], [24], [14] adapted to the needs of the ISC method.

4.1. Test modes

We have studied in [14] drift type test modes on turbulent plasmas. The frequencies and the growth rates are obtained as functions of the characteristics of the turbulence. They show that ion diffusion (generated by the random component of the trajectories) has a stabilizing effect, while ion trapping (the quasi-coherent component) leads to strong nonlinear effects: increase of the correlation lengths, nonlinear damping of the drift modes and generation of zonal flow modes. The strength of each of these processes depends on the parameters of the turbulence.

We use the basic description of the (universal) drift turbulence provided by the drift kinetic equation in the collisionless and low density limit. We consider a plasma confined by an uniform magnetic field B, taken along the $\mathbf{e}_3$ axis in a rectagular system of coordinates. The density gradient with characteristic length L_n is taken along $\mathbf{e}_1$. The drift wave instability that is produced by the electron kinetic effects and the ion polarization drift velocity is studied. The solution of the dispersion relation for quiescent plasma is (see [37])

$$\omega = \frac{k_2 V_*}{1 + k^2 \rho_s^2}, \quad \gamma = \gamma_0 \omega \left(k_2 V_* - \omega \right) \tag{18}$$

where ω is the frequency of the mode with wave number $\mathbf{k} = [k_1,\ k_2,\ k_z]$, $k = \sqrt{k_1^2 + k_2^2}$, $\mathbf{V}_* = V_* \mathbf{e}_2$, $V_* = T_e/(eBL_n) = \rho_s c_s / L_n$ is the diamagnetic velocity, $\rho_s = c_s/\Omega_i$, $c_s = \sqrt{T_e/mi}$, T_e is the electron temperature, m_i is the ion mass, e is the absolute value of electron charge and $\Omega_i = eB/m_i$ is the ion cyclotron frequency. The constant γ_0 that plays the role of drive of the instability is $\gamma_0 = \sqrt{\pi/2} / \left(|k_z| \, v_{Te} \right)$, where $v_{Te} = \sqrt{T_e/m_e}$.

Electron and ion responses to a small perturbation $\delta\phi$ applied on the turbulent state with potential ϕ are determined. They lead to a modified propagator

$$\overline{\Pi}^i = i \int_{-\infty}^{t} d\tau \ M(\tau) \ \exp\left[-i\omega \left(\tau - t \right) \right], \tag{19}$$

which includes the effects of the turbulence in the function $M(\tau)$ defined by

$$M(\tau) \equiv \left\langle \exp\left[i\mathbf{k} \cdot \left(\mathbf{x}(\tau) - \mathbf{x} \right) - \int_{\tau}^{t} d\tau' \ \nabla \cdot \mathbf{u}_p \left(\mathbf{x}(\tau') \right) \right] \right\rangle, \tag{20}$$

where the average $\langle\rangle$ is over the ion trajectories in the stochastic potential ϕ. The polarization drift $\mathbf{u}_p$ determines a compressibility term due to its divergence $\nabla \cdot \mathbf{u}_p = -\partial_t \Delta\phi / \left(\Omega_i B \right)$. The dispersion relation (quasineutrality condition) is the same as in the quiescent plasma in terms of the propagator

$$- \left(k_y V_{*e} - \omega \rho_s^2 k_\perp^2 \right) \overline{\Pi}^i = 1 + i \sqrt{\frac{\pi}{2}} \frac{\omega - k_y V_{*e}}{|k_z| \, v_{Te}} \tag{21}$$

(see [14] for details).

The spectrum of the potential ϕ is modeled in accord with the characteristics of the drift type turbulence. It is zero for $k_2 = 0$ because the drift modes are stable, and

it has two symmetrical peaks for $k_2 = \pm k_0$

$$S(\mathbf{k}) \sim k_2^m \exp\left(-\frac{k_1^2}{2}\lambda_1^2\right)\left[\exp\left(-\frac{(k_0-k_2)^2}{2}\lambda_2^2\right) - \exp\left(-\frac{(k_0+k_2)^2}{2}\lambda_2^2\right)\right]. \quad (22)$$

The Fourier transform gives the EC

$$E(\mathbf{x},t) = \Phi^2 \partial_y^m \left[\exp\left(-\frac{x_1^2}{2\lambda_1^2} - \frac{x_2'^2}{2\lambda_1^2}\right)\frac{\sin k_0 x_2'}{k_0}\right], \quad (23)$$

where $x_2' = x_2 - V_{*e}t$ accounts for the motion of the drift turbulence potential with the diamagnetic velocity. The spectrum and the EC are functions of five parameters: Φ, λ_1, λ_2, k_0 and the power m that determines the decay of the spectrum to $k_2 = 0$.

The ISC method shows that the evolution of the drift turbulence is in good agreement with the model (22) of the spectrum (see Section 8).

The statistics of the ion trajectories in turbulence with the spectrum of the type (22) is discusses in the next subsection. The micro-probability of the displacements can be Gaussian or non-Gaussian, depending on the spectrum parameters and on the decorrelation time τ_d. More precisely, the statistics depends on the fraction of trapped ions n_{tr} and on the sizes s_1, s_2 of the structure of trajectory that appear due to trapping. The most complex case corresponds to n_{tr} comparable to the fraction of free trajectories $n_f = 1 - n_{tr}$. It is characterized by the existence of ion flows determined by ion trapping in the moving potential. The micro-probability splits in two parts that move in opposite directions. The trapped trajectories drift with the potential and have the velocity V_* and the free trajectory have the velocity $V_f = -nV_*$ that ensures zero ion flux (here $n = n_{tr}/n_f$).

The simple approximation (33) (discussed in the next Section) includes the main features of the micro-probability. It has the advantage of enabling the derivation of simple analytical expressions for the function M (20), the renormalized propagator (19) and eventually to solve the dispersion relation (21) for the complex frequency of the drift modes (see [14]).

The drift modes have modified frequency and growth rate compared to the quiescent plasmas (18), which depend on the characteristics of the trajectory structures and on the diffusion coefficients

$$\overline{\omega}_d = \frac{1}{2}\left[\overline{\omega}_0 + (1-n)\,\overline{k}_2 + sg\sqrt{\overline{\omega}_n^2 + \frac{4n\overline{k}_2^2}{1+\mathcal{F}\overline{k}^2}}\right], \quad (24)$$

$$\overline{\gamma}_d = \frac{\overline{\gamma}_0\left(\overline{\omega}_d + n\overline{k}_y\right)\left[(1-n)\,\overline{k}_y - \overline{\omega}_d\right] - n_f\overline{k}_i^2\overline{D}_i}{\left[(1-n)\,\overline{k}_y - \overline{\omega}_d\right]^2\left(1+\mathcal{F}\overline{k}_\perp^2\right) + n\overline{k}_y^2}\left(\overline{k}_y - \overline{\omega}_d\right)^2, \quad (25)$$

where $\overline{\omega}_n = \overline{\omega}_0 + (n-1)\,\overline{k}_2$, $\overline{\omega}_0 = \mathcal{F}\overline{k}_2/\left(1+\mathcal{F}\overline{k}^2\right)$ is the frequency obtained for $n \to 0$, $\mathcal{F} = \exp\left(-s_i^2 k_i^2/2\right)$ is a factor that depends on the sizes of the trajectory structures,

$sg = sign\,(\overline{\omega}_n)$ and $\overline{\gamma}_0 = \gamma_0 c_s/L_n$. Usual normalized quantities $\overline{k}_i = k_i\rho_s$, $\overline{\omega} = \omega L_n/c_s$, $\overline{\gamma} = \gamma L_n/c_s$ are used.

The compressibility term determines unstable modes completely different from the drift modes. They have $k_y = 0$ and very small frequencies

$$\overline{\omega}_{zf} = -\overline{k}_x\overline{a}\frac{1+\mathcal{F}\overline{k}_x^2 n_f}{1+\mathcal{F}\overline{k}_x^2}, \tag{26}$$

$$\overline{\gamma}_{zf} = \frac{n_{tr}\mathcal{F}\overline{k}_x^2\left[\overline{\gamma}_0\overline{\omega}_{zf}^2 - n_f\mathcal{F}\overline{k}_x^4\overline{D}_x\right]}{\left(1+n_f\mathcal{F}\overline{k}_x^2\right)\left(1+\mathcal{F}\overline{k}_x^2\right)}, \tag{27}$$

where $\overline{a} = a/V_*$. These unstable modes that are named zonal flow modes are the consequence of trapping combined with the polarization drift. The compressibility term in the function M determines correlations with the displacements

$$L_i(\tau) = -\frac{1}{\Omega_i B}\int_\tau^t d\tau'\,\langle x_i\,(t)\;\;\partial_{\tau'}\Delta\phi\,(\mathbf{x}(\tau'))\rangle\,, \tag{28}$$

which, as evaluated in [14], can be significant for $i = 1$ (in the direction of the density gradient) for the trapped ions. It can be approximated by

$$L_1(\tau,t) \cong a\,(t-\tau)\,,\quad a = 2\partial_y^2\Delta E(\mathbf{0})\frac{\tau_{fl}V_*}{\Omega_i B^2}. \tag{29}$$

This correlation determines an average velocity for the trapped ions. One can see that when trapping is negligible ($n_{tr} \cong 0$), $\omega_{zf} = -k_x a$ and $\gamma_{zf} = 0$, and that $\omega_{zf}, \gamma_{zf} = 0$ for $\overline{a} = 0$.

4.2. Test particles

The EC of the drift turbulence (23) has a special shape determined by the absence of the modes with $k_2 = 0$ in the spectrum (22). It has negative parts and possibly an oscillating decay as shown in Figure 8b. This leads to a transport process with important differences compared to the examples presented in Section 3.2 that are obtained for a monotonically decreasing EC. The transport coefficients in this type of EC were studied in [25], [24] for ion and electron diffusion.

We determine here the parameters required by the test mode study and present a short review of the diffusion process.

The equation for the trajectories in the drift turbulence with a zonal flow mode potential ϕ_{zf} (in the frame that moves with the potential) is

$$\frac{dx_i}{dt} = -K_*^{'}\varepsilon_{ij}\partial_j\left[\phi(\mathbf{x},t) + Z\;\phi_{zf}(\mathbf{x},t)\right] + V_d, \tag{30}$$

where dimensionless quantities are used with the units: ρ_s (for the distances and the correlation lengths λ_i, λ_{zf}), $\tau_0 = L_n/c_s$ (for time) and Φ (for the potential). In this

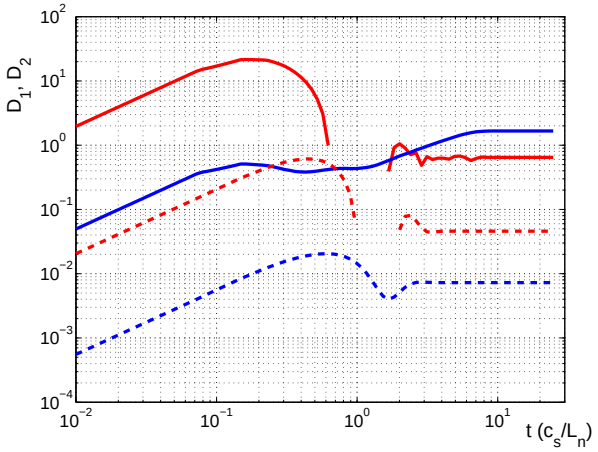

Figure 3. Exemples of diffusion coefficients in drift turbulence: $D_{11}(t)$ (red) and $D_{22}(t)$ (blue) in the quasilinear (dashed lines for $K_*^{'} = 0.5$) and nonlinear (continuous lines for $K_*^{'} = 5$) regimes. The other parameters are $k_1^0 = 2.5$, $\lambda_1 = 2$, $\lambda_2 = 1$, $V_d = 1$ and $\tau_d = 5$.

normalization, the time flight is a decreasing function of Φ, while τ_* and τ_d are fixed (independent of the turbulence amplitude). The normalized amplitude of the zonal flows is $Z = \Phi_{zf}/\Phi$ and the normalized diamagnetic velocity is $V_d = 1$. The dimensionless parameter $K_*^{'}$ is the measure of turbulence amplitude

$$K_*^{'} \equiv \frac{\Phi}{B\rho_s V_*} = \frac{e\Phi}{T_e}\frac{L_n}{\rho_s}.$$

This parameter can be written as $K_*^{'} = K_* L_n/\rho_s$, which shows that it is proportional to the Kubo number that describes the decorrelation by an average velocity $K_* = V_2/V_*$. As shown in [25], the transport regimes depend only on K_*, which includes both the effects of the turbulence and of the average velocity.

Typical results for the diffusion coefficients are shown in Figure 3. We note that the transport is not isotropic. The amplitudes of the velocity components are different for the EC (23). The special shape of the EC leads to diffusion regimes for D_1 that have similar dependence on the decorrelation time in the quasilinear and nonlinear regime. This determines smaller values of the quasilinear D_1 than in a decaying EC. The shape of the EC also determines negative parts in the time dependence of $D_{11}(t)$ (seen as breaks in the red lines in Figure 3). The modification of D_2 appears in the quasilinear regime too, and consists of significant decrease, as seen by comparing the dashed blue curves in Figures 3 and 2.

A large increase of the asymptotic coefficient D_2 appears at the transition from the quasilinear to the nonlinear regime, which provides a strong auto-control parameter. As seen in Figure 3, the ratio of the asymptotic values in the nonlinear and quasilinear regime is much larger for D_2 than for D_1.

The parameters of the trajectory structures are obtained using the DTM as weighted averages of the decorrelation trajectories $\mathbf{X}^S(t)$ in the static potential. The

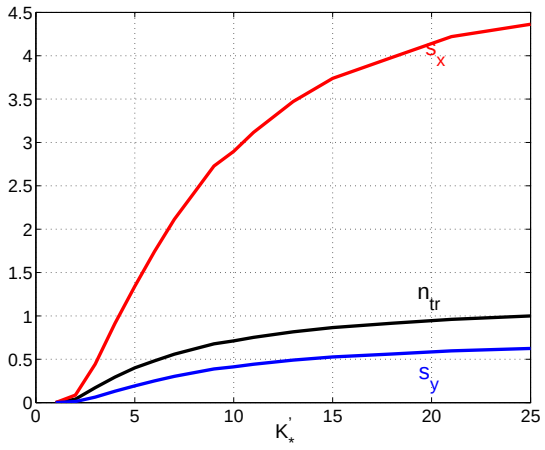

Figure 4. The characteristics of the trajectory structures as functions of the normalized amplitude of the potential $K_*^{'}$: the fraction of trapped ions (black) and the size of the structures s_x (red), s_y (blue). The other parameters are as in Figure 3.

solutions of Eq. (17) are periodic functions in this case with the periods $T(\phi^0, \mathbf{v}^0)$ that depend on the subensemble. The fraction of trapped trajectories at time t is

$$n_{tr}(t) = \int d\phi^0 P(\phi^0) \int dv_1^0 dv_2^0 P(v_1^0) P(v_1^0)\ c_{tr}(t; \phi^0, \mathbf{v}^0), \tag{31}$$

where $c_{tr}(t; \phi^0, \mathbf{v}^0) = 1$ if $t > T(\phi^0, \mathbf{v}^0)$ and $c_{tr}(t; \phi^0, \mathbf{v}^0) = 0$ if $t < T(\phi^0, \mathbf{v}^0)$. The sizes of the trajectory structures in the two directions are

$$s_i(t) = \int d\phi^0 P(\phi^0) \int dv_1^0 dv_2^0 P(v_1^0) P(v_1^0)\ X_i^{\max}(t; \phi^0, \mathbf{v}^0), \tag{32}$$

where $X_i^{\max}(t; \phi^0, \mathbf{v}^0)$ is the dimension of $\mathbf{X}^S(t; \phi^0, \mathbf{v}^0)$ along the direction i if $t > T(\phi^0, \mathbf{v}^0)$ and $X_i^{\max}(t; \phi^0, \mathbf{v}^0) = 0$ if $t < T(\phi^0, \mathbf{v}^0)$.

The functions $n_{tr}(t)$ and $s_i(t)$ describe the growth of the trajectory structures. These functions saturate in a time τ_s, which is the characteristic time for the formation of the structure. τ_s is an increasing function of the amplitude of the turbulence $K_*^{'}$. The asymptotic values of $n_{tr}(t)$ and $s_i(t)$ describe the parameters of the structures as functions of the characteristics of the turbulence. The dependence on the amplitude of the turbulence is presented in Figure 4. It shows that the structures continuously increase when turbulence amplitude increases and eventually they include all the trajectories $n_{tr} \to 1$. In the presence of a decorrelation process with characteristic time $\tau_d < \tau_s$, the parameters of the structures are smaller because they are destroyed during the formation at the time τ_d. They can be approximated by $n_{tr}(\tau_d)$ and $s_i(\tau_d)$, instead of the asymptotic values.

The micro-probability $P^{\tau_d}(\mathbf{x}, t)$ can be evaluated using the DTM as a histogram of the decorrelation trajectories. It can be Gaussian, or non-Gaussian, depending on turbulence parameters and on the decorrelation time τ_d. Non-Gaussian P^{τ_d} are

associated to the presence of trapping. The micro-confinement appears very clearly in the probability as a narrow peak in $\mathbf{x} = \mathbf{0}$, which remains invariant after a formation time τ_s, the same as in the time evolution of the fraction of trapped trajectories $n_{tr}(t)$. P^{τ_d} has also a time dependent part around this maximum, which is determined by the free particles. For the drift turbulence case, the motion of the potential with the diamagnetic velocity leads to the separation of the two parts of the micro-probability: the narrow peak is displaced in the direction $V_d\mathbf{e}_2$ and the free particle part concentrates in the opposite direction then moves. This result is in qualitative agreement with the process of flow generation in zero divergence velocity fields (Section 2), but the flow velocities obtained with the DTM are smaller than (2).

The analytical results for the test modes (Section 4.1) are obtained using simplified approximations of P^{τ_d} in agreement with Eq. (2) for the ion flows (see [14] for details). The trapped particle part was represented for simplicity by a Gaussian function, but with fixed dispersion given by the size s_i of the structures $S_i = s_i^2$. The shape of this function does not change much the estimations. The free trajectories are described by a Gaussian with dispersion that grows linearly in time: $S_i'(\tau) = S_i + 2D_i(t - \tau)$, $i = x, y$. The initial value $S_i'(t) = S_i$ is an effect of trapping. It essentially means that the trajectories are spread over a surface of the order of the size of the trajectory structures when they are released by a decorrelation mechanism. Introducing the flows (2), the approximation for the micro-probability is

$$P^{\tau_d}(x, y, t) = n_{tr}G(x, y - V_d t; \mathbf{S}) + n_f G(x, y - V_f t; \mathbf{S}'), \tag{33}$$

where $G(\mathbf{x}; \mathbf{S})$ is the 2-dimensional Gaussian distribution with dispersion $\mathbf{S} = (S_x, S_y)$. We note that this probability is non-Gaussian.

The separation of the distribution and the existence of ion flows in drift type turbulence are confirmed by numerical simulations [20].

5. The iterated self-consistent method

The idea of the iterated self-consistent (ISC) method is based on the difference between the description of turbulence evolution and the mode representation. One can define in the evolution equation characteristic times for each process (represented by a term in the equation). The ordering of these characteristic times shows which are the processes that have important contributions at a given stage of evolution. Neglecting the small terms leads to simplified equations that give the short time evolution, for time smaller than the characteristic times of the neglected terms. The estimation of the characteristic times provides the basis for a systematic approximations that can strongly simplify the evolution equation at small time. On the other side, the mode representation of turbulence does not deal with time evolution but it determines the possible frequencies and wave numbers that are supported by the system and their tendency of amplification or damping. These quantities include effects of processes that are negligible at short time.

The combination of the study of test modes on turbulent plasma with the evaluation of the short time equilibrium of the distribution functions can provide a much simplified approach and even the possibility to develop a semi-analytical approximate method for the turbulence evolution.

More precisely, the short time solution is an approximation that is not valid at large times where the neglected small terms in the evolution equation determine the accumulation of significant effects. These effects are taken into account using the test modes. The frequency and the growth rate of a small perturbation $\delta\phi$ of the background potential ϕ include the terms and the corresponding effects that are neglected in the small time equilibrium distribution. The effective calculation of these characteristics of the modes requires the statistics of the trajectories (for evaluating the average propagator). The diffusion coefficients and the probability of displacements depend on the momentary Eulerian correlation of the background potential. The latter is provided by the small time solutions of the evolution equations. Finally, the frequencies and the growth rates of all modes determine the evolution of the background potential.

Thus the methodology of the ISC approach consists of repeated steps that contain the following calculations.

- The evaluation of approximate (short time) equilibrium distribution functions in the presence of background turbulence and of the Eulerian correlation of the potential.
- The calculation of the statistical characteristics of the trajectories (diffusion coefficients, probability of displacements, characteristics of the quasi-coherent structures) as functions of the Eulerian correlation of the potential. This is one of the main modules, presented in Section 4.2.
- The calculation of the renormalized propagator (averaged over trajectories) and evaluation of the frequencies and the growth rates of the test modes. This is the second main module of the ISC.
- The evolution of the spectrum on a small time interval is obtained using the growth rates of all modes. It is the starting point of a new step in this iterated method.

In the case of the drift instability studied here [37], the small time distributions are the adiabatic response for the electrons and $f_0^i = n_0(x_1)F_M^i\,(1 + e\phi(\mathbf{x} - V_d t\mathbf{e}_2)/T_e)$ for the ions, where $n_0(x_1)$ is plasma density, V_d is the diamagnetic velocity and F_M^i is the Maxwell distribution of ion velocities. They correspond to the stable drift waves and show that an arbitrary potential ϕ in a nonuniform plasma drifts with the diamagnetic velocity. The neglected terms are taken into account in the linearized equation for the small perturbation. The kinetic effects of the electrons determine their nonadiabatic response, which is the drive of the instability. This response is the same as in quiescent plasmas due to the fast parallel motion of the electrons. The compressibility effects determined by the polarization drift of the ions make the growth rates positive. The stochastic ion trajectories in the background potential ϕ, which can become rather complex by acquiring coherent aspects at large amplitudes of ϕ, change the frequencies and the growth rate leading to strong nonlinear effects in the evolution of turbulence.

Several important simplification can be operated in methodology of the ISC method. The most important concern the test mode module that is practically eliminated in the present case by the analytical results available for the frequencies and the growth rates of drift and zonal flow modes in turbulent plasmas (Section 4.1). Moreover, we have found that the spectra of the drift and zonal flow components obtained in the iterated evolution can be approximated by expressions of the type of Eq. (22). It is thus sufficient to determine the parameters in this expression at each step. This permitted to have analytical expressions for the EC in the test particle module.

A computer code was developed for the study of the drift turbulence using the ISC method. We note that this code is not performing the simulation of the turbulence, but it calculates the quantities related to test particles and test modes according the iterated procedure presented here. The run time is of few hours on a laptop.

6. Drift turbulence evolution

There are two possible mechanisms for the attenuation of the drift turbulence.

The first is the diffusive damping, which can be strongly enhanced due to the increase of D_2 in the nonlinear regime. The process is produced by the diamagnetic velocity that modifies the total potential producing bundles of open contour lines with average orientation along its direction. The zonal flow modes can contribute to this process since they provide an additional component along $V_d\mathbf{e}_2$ [25]. This velocity is stochastic with zero average, but it determines an average effect due to the nonlinear dependence of n_{tr} on V_d (Figure 4).

The second mechanism is the non-linear self-damping determined by the ion flows. The increase of the rate of trajectory trapping $n = n_{tr}/(1 - n_{tr})$ determine the decrease of γ_d, which becomes negative for all values of the wave numbers at $n = 1$, as results from Eq. (25).

The self-consistent evolution is expected to be much more complicated since the processes identified by a separate analysis of the two main modules can be simultaneous present or they can combine in a synergistic way. Moreover, there are other parameters that are included in both modules (the correlation lengths, the dominant wave numbers, the size of the trajectory structures) that change during the evolution and can strongly affect the quasi-coherent structures.

We have found two types of evolution depending on the strength of the drive of the instability $\overline{\gamma}_0$. The evolution at small drive (small $\overline{\gamma}_0$ that corresponds to large k_z) is controlled by the diffusion. At high drives that appear for smaller k_z, the effects of trajectory trapping become dominant. In both cases, there is a similar initial stage.

The evolution of drift turbulence is analyzed below. We use in the figures red and blue colors for the two-dimensional quantities (red for the direction $\mathbf{e}_1$ of the density gradient and blue for the direction $\mathbf{e}_2$) and black for the scalar functions or for the zonal flows.

6.1. The initial stage

The evolution of turbulence has an initial stage that depends on the initial condition for the spectrum. However, for all physically reasonable conditions, the shape of the spectrum changes and it always develops two symmetrical maxima in $k_1 = 0$ and $k_2 = \pm k_0$. They are produced by the diffusive damping of the modes, which acts very strongly on large k_2 and $k_1 \cong 0$ domain and makes $\gamma < 0$ even at small values of the diffusion coefficient D_y. The diffusive decay at large $|k_2|$ combined with the growth rate that decay to zero at small $|k_2|$ determine the generation of the two peaks in the spectrum. This leads to the increase of the anisotropy of the turbulence. The amplitude of the normalized velocity V_1 increases while V_2 decreases in this stage (see the small time evolution in the Figures 5a and 6a). The cause of this behaviour is the increase of the dominant wave number k_2^0 and of the correlation lengths λ_i (Figures 5b and 6b). The amplitude of the potential fluctuations represented by $K_*^{'}$ increases exponentially.

It is interesting to note that, besides the large stochastic velocity along the density gradient ($V_1 \gg V_2$), the diffusion coefficient is smaller ($D_1 > D_2$). This behavior is the effect of the special shape of the EC of the drift turbulence that yields decreasing diffusion coefficient D_1 at large τ_d even in the quasilinear regime.

The initial stage is not a regime of completely independent evolution of the modes. The influence of the background turbulence that consists of the diffusive damping is not negligible at the very small values that correspond to this stage. Namely, the growth rate in the quasilinear limit that can be obtained from Eq. (25) for $n = 0$ and $\mathcal{F} = 1$ at $k_1 = 0$ is

$$\overline{\gamma}_d = \overline{k}_2^2 \left(\gamma_0 \frac{\overline{k}^2}{(1+\overline{k}^2)^2} - \overline{D}_2 \right).$$

The parentheses becomes negative at large enough $\overline{k}$ because the first term decays to zero.

6.2. Evolution at weak drive

Typical evolution at weak drive is presented in Figure 5, where $\overline{\gamma}_0 = 1$. After the initial stage, the diffusive damping becomes stronger and it determines important changes in the evolution. The amplitude of the potential $K_*^{'}$ continuous to increase but with a slower rate: the exponential evolution is replaced by a roughly linear increase (Figure 5a, the back curve for $K_*^{'}$). Both components of the normalized velocity decrease. They have a fast decay followed by the tendency of saturation (Figure 5a). This is the effect of diffusional damping. The diffusion coefficients increase as $\left(K_*^{'}\right)^2$ and they produce the decrease of the growth rate of the drift modes.

Besides this well known effect of damping, the diffusion determines significant changes of the shape of the spectrum. The width of the two peaks decreases on both directions, which determines the increase of the correlation lengths. It also determines the displacement of the position of the peaks toward smaller wave numbers. The

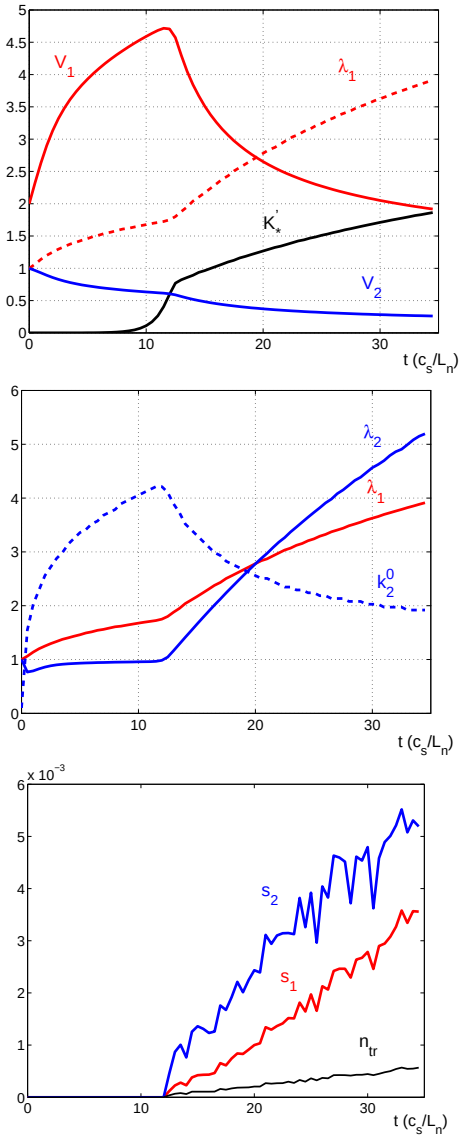

Figure 5. Drift turbulence evolution for weak drive. a) The turbulence amplitude parameter $K_*^{'}$ (black line) compared to the nonlinear limit λ_1. The components of the normalized velocity are also plotted (red and blue curves). b) The parameters of the EC. c) The trajectory structure sizes s_1, s_2 and the fraction of trapped trajectories n_{tr}.

evolution of the spectrum parameters is shown in Figure 5b.

The condition for the transition to the trapping regime ($K_*^{'} > \lambda_1$) is not attained in this case since, as seen in Figure 5a, the increase rate is larger for λ_1 than for $K_*^{'}$. The structures of trajectories are practically absent, as seen in Figure 5c where $n_{tr} < 10^{-3}$ and the $s_i < 10^{-2}$.

Drift turbulence evolution at weak drive is essentially determined by ion diffusion, which reduces the growth rate and determines a significant change of the spectrum that prevents the development of the coherent effects produced by trapping.

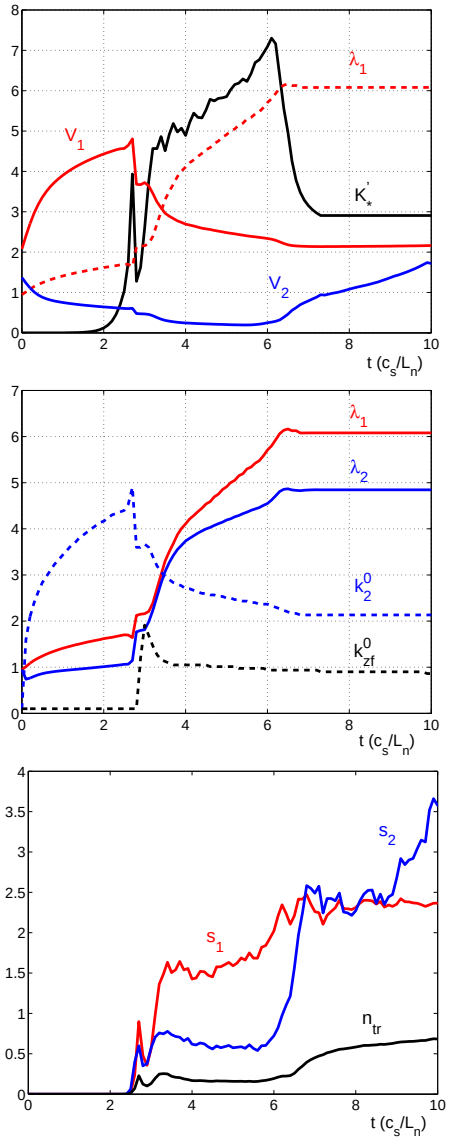

Figure 6. The same as in Figure 5, but for the evolution of drift turbulence with strong drive. The dominant wave number of the zonal flow modes is shown in b (black dashed line).

6.3. Evolution at strong drive

The increase of the drive parameter determines a strong effect on turbulence evolution, as seen in Figures 6-8, where $\overline{\gamma}_0 = 5$. This large values of $\overline{\gamma}_0$ lead, since the initial stage of the evolution, to a faster increase of the amplitude of the normalized potential $K_*^{'}$. Ion diffusion determines the same effects as in the weak drive case, but the fast exponential increase of the potential up to larger values makes $K_*^{'} > \lambda_1$, and determines ion trapping.

Three time intervals with different characteristics of the evolution can be identified in the typical example presented in Figure 6: $t < 2.5$, $2.5 < t < 6$ and $t > 6$. The first interval corresponds to the initial stage of quasi-independent development of the modes.

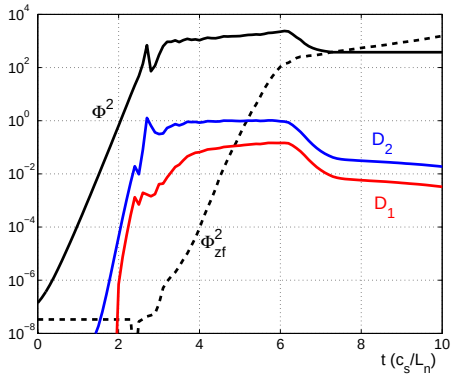

Figure 7. Evolution of the amplitude of the drift and zonal flow modes compared with the evolution of the diffusion coefficients.

The other two intervals are influence by the trapping process but in different ways.

As seen in Figure 6a, the evolution enters in the nonlinear regime $K_*^{'} > \lambda_1$ at the end of the initial stage determining ion trajectory trapping (Figure 6c). The potential $K_*^{'}$ has a fast transitory decay, followed by a regime of continuous increase of the average $K_*^{'}$ (Figure 6a, black curve). During this stage, $K_*^{'} > \lambda_1$ and both parameters increase with roughly the same rate. The ratio $K_*^{'}/\lambda_1$ is approximately constant, which corresponds to small variation of the parameters of the trajectory structures (Figure 6c, the time interval $[4,\ 6]$). The spectrum and the EC are strongly modified during this interval. The correlation lengths λ_i increase significantly and the dominant wave number k_2^0 decreases (Figure 6b). The evolution of the velocity is different from that of the potential as reflected in the normalized velocities $V_1,\ V_2$, which are time dependent functions (see Figure 6a). Their evolution is actually determined by the change of the characteristics of the EC, because $V_1^2 \cong (k_2^0)^2 + 3/\lambda_2^2$ and $V_2^2 \cong 1/\lambda_1^2$.

A different evolution regime appears at $t > 6$ in the example presented in Figure 6. The normalized potential drops and it saturates (Figure 6a). The normalized velocity V_1 saturates and V_2 increases. The characteristics of the EC, λ_i and k_2^0, also saturate (Figure 6b). The condition for the existence of trajectory structures is no more fulfilled ($K_*^{'}$ is significantly smaller than λ_1). However, trapping becomes much stronger (n_{tr} and the size of the structures increase, as seen in Figure 6c).

This rather nontrivial evolution of the drift turbulence can be understood by analyzing the nonlinear effects that influence the growth rate (25): the ion diffusion, the formation of ion trajectory structures and flows.

The evolution of the diffusion coefficients D_i is presented in Figure 7, where the amplitudes of the drift turbulence Φ^2 and of the zonal flow potential Φ_{zf}^2 are also shown. One can see that the zonal flow modes become unstable when trapping appears and they grow exponentially until $t \cong 6$. Their amplitude is negligible compared to that of the drift turbulence during this time interval. Thus, it is not expected an important role of the zonal flow modes at this stage.

The diffusion coefficient D_2 is much larger than D_1. It has a very large increase

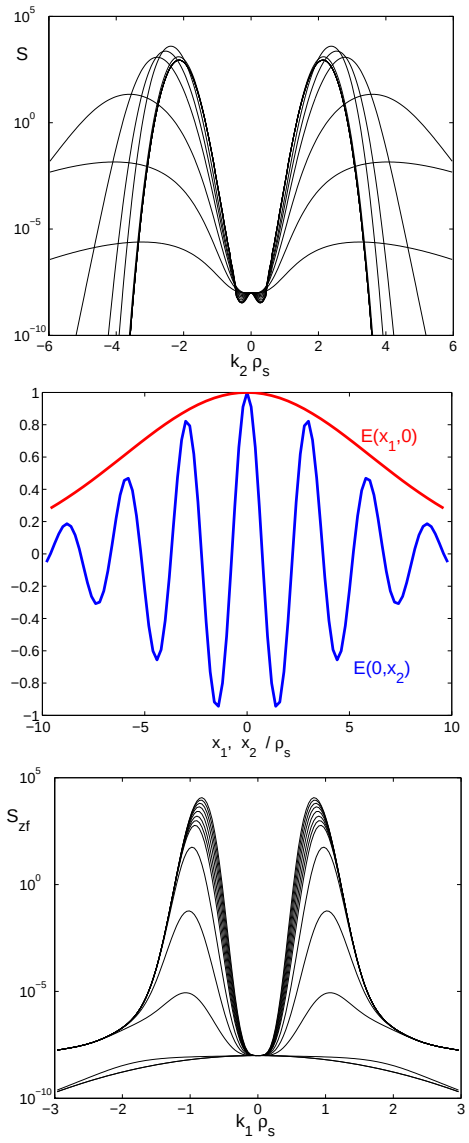

Figure 8. The spectrum (a) and the EC (b) of the drift turbulence and the spectrum of the zonal flow modes (c). The spectra are plotted at time intervals $\delta t = L_n/c_s$ and the EC is at $t = 9L_n/c_s$.

rate during the first transition into the nonlinear regime. The cause is ion trapping in the potential that drifts with the diamagnetic velocity, which determines a strong amplification of the diffusion along $V_d\mathbf{e}_2$, as discusses in Section 4.2 and represented in Figure 3. The strong diffusion determines the transitory decay of the potential $K_*^{'}$ under the nonlinearity limit. Consequently, the structures of the ion trajectories are destroyed. The fraction of trapped trajectories and the size of the structures decrease when $K_*^{'}$ decreases (Figure 4). The diffusion coefficient D_2 decreases due to both effects (the decrease of Φ and the reduction of structures). One can see in Figures 7 and 6c that transitory peaks and decays appear around $t = 2.7$ for D_2, Φ, n_{tr} and s_i. After that, the potential increases again and reaches a higher level in the nonlinear regime. The

diffusion coefficients D_2 recovers large values, but without driving the decay process. The strong diffusion is supported by the potential, which increases at this stage instead of having a fast decay as in the previous event. The cause of the different behahiour is the evolution of the parameters of the spectrum. The dominant wave number k_2^0 (maxima of the spectrum) and the width of the spectrum $\delta k_i \cong \sqrt{2\pi}/\lambda_i$ decrease as seen in Figure 6b. As a consequence, the damping effect of the diffusion $k_i^2 D_i$ is weaker at small wave numbers and the growth rate of the modes remains positive.

The third time interval in the evolution is characterized by the presence of the zonal flow modes at amplitudes comparable to Φ. The drift turbulence decays and saturates while the zonal flow amplitude increases. The EC of the drift potential also saturates (λ_i and k_2^0 are roughly constant during this interval). The increase of V_2 shown in Figure 6a is determined by the growing contribution of the zonal flow modes.

Zonal flow provide the explanation for the increase of trapping (Figure 6c) that seems paradoxical in the condition of the decay of $K_*^{'}$ below the nonlinearity limit. The structure of the potential contour lines is modified by the zonal flow potential, which determines larger structures that capture the ions which are not micro-confined by the drift turbulence. The fraction of trapped ions and the size of the structures increase in correlation with the increase of Φ_{zf} (Figures 6c and 7). A deformation of the trajectory structures appears due to the stronger increase of s_y that of s_x. They are initially elongated in the gradient direction and eventually they acquire a shape dominated by the zonal flow modes. The fraction of trapped ions strongly increases and, at $t \cong 7$, it overcomes the value $n_{tr} = 1/2$ ($n = 1$) that corresponds to negative growth rate of the drift modes (25) even in the absence of diffusion.

The diffusion coefficients decrease in this stage due to the decay of the potential Φ. The increase of the diffusion D_2 determined by the zonal flow contribution discussed in [25] is not observed here because the negative growth rate effect leads to the transition in the quasilinear regime and the condition ($\Phi_{zf} = \Phi > \lambda_1$) for this effect is not fulfilled. The decay of the drift turbulence is caused by the zonal flow modes through the amplification of trapping rather than by an increased diffusion.

The evolution of the spectrum of the drift turbulence is presented in Figure 8a, which shows the function $S(0, k_2)$ at time intervals $\Delta t = 1$. The spectrum becomes narrower as time increases and its maxima move to smaller values of k_2.

The Eulerian correlation of the potential is shown in Figure 8b. The oscillatory dependence on x_2 is determined by the narrow peaks of the spectrum. It determines the small diffusion along the density gradient $D_1 < D_2$ despite the amplitude of the stochastic velocity that is much larger in this direction ($V_1 > V_2$).

The spectrum of the zonal flow modes $S_{zf}(k_1)$ is shown in Figure 8c at the same time moments as $S(0, k_2)$. The two spectra have similar shapes, with the difference that the zonal flow modes have small tails at large k_1 while a very strong cut appears for the drift modes at large k_2. This is the consequence of the diffusive damping that is weak in the case of the zonal flow modes, as seen in Eq. (27). The dominant wave number of the zonal flow modes is around $k_{zf} \cong 1$, and it has a weak decrease with time (as also

seen in Figure 6b, black curve).

7. Summary and conclusions

Particle trajectories in 2-dimensional incompressible velocity fields can include both random and coherent aspects, which appear as random sequences of large jumps and trapping or eddying events. This complex behaviour is determined by the Hamiltonian structure of the equation of motion, and it effectively appears when the stochastic potential is only weakly perturbed. The trapped trajectories have a high degree of coherence and they form intermittent quasi-coherent trajectory structures. Their size and life-time depend on the characteristic of the turbulence. The distribution of the displacements is non-Gaussian in the presence of these vortical structures. We have developed semi-analytical statistical methods for the study of such complex trajectories, the DTM [12] and the NSA [13]. It was shown that these methods provide very clear physical images on the nonlinear transport processes and reasonably good quantitative results.

The quasi-coherent structures, which actually produce a process of micro-confinement, have strong effects on the transport. The transport is determined by the long jumps, while the structures represent a diffusion reservoir, which leads to significant increase of the diffusion coefficients when the particles are released by a decorrelation mechanism. The transport process is completely different in the presence of structures in the sense that the dependence on the parameters is different.

The quasi-coherent structures have strong effect on the test modes on turbulent plasmas. This conclusion is drawn from an analytical study of the drift turbulence that includes the coherent aspects of the trajectories beside the random ones [14]. The frequencies and the growth rates of the test modes on strongly turbulent plasmas could be determined by the renormalized propagator procedure. A different perspective on important aspects of the physics of drift type turbulence in the strongly nonlinear regime is deduced. The main role in the nonlinear processes is shown to be played by the ion trajectory structures. The nonlinear damping of drift modes and the generation of zonal flow modes appear when trapping is strong due to the ion flows generated by the drift of the potential with the diamagnetic velocity. The conclusion drawn from this test mode study is that there is no causality relation between these processes, although there is time correlation between them. The predator-prey paradigm is not sustained by these results.

These test particle and test mode studies determine the transport coefficients and the characteristics of the test modes for given statistical description of the turbulence, as functions of turbulence parameters. The conclusions on turbulence and transport evolution base on the analysis of these results are speculative, because they only suppose that the positive growth rates of the test modes eventually drive the turbulence in the nonlinear regime.

We show here that test particle and test mode studies can be connected in an

iterated self-consistent (ISC) theoretical description of turbulence evolution. It is an approximate Lagrangian method that takes into account the quasi-coherent aspects of particle trajectories in turbulence. A computer code based on the ISC was developed for the drift turbulence in uniform magnetic field. The advantage of this approach is the clear physical image that can be deduced for complicated nonlinear processes. They are related to the basic problem of particle advection in turbulence.

The first results show that drift turbulence evolution can have different characteristics, which essentially depend on the drive parameter.

In the case of weak drive of the drift turbulence, the evolution is determined by the nonlinear effects of the ion diffusion. They consist not only of the diffusive damping that reduces the growth rate of the modes, but also of the modification of the spectrum. The dominant wave number decreases and the correlation length increase. In particular the increase of λ_1 leads to values that are larger than those of the normalized potential $K_*^{'}$ during the evolution, which shows that trajectory trapping is negligible. The ion trajectories are random in this case, with negligible structures.

In the case of strong drive, both random and the quasi-coherent characteristics of the trajectories are generated during the evolution. The structures of trajectories influence the evolution of the drift turbulence by three mechanisms. All of them are connected to the quasi-coherent trajectory structures. One in the dependence of the growth rates of the test modes (25) on the parameters of the structures (the fraction of trapped trajectories n and the size of the structures). The increase of n and of s_i determine the decrease of $\overline{\gamma}_d$, which become negative for all wave numbers at $n = 1$ even for $D_i = 0$. The increase of the structures determines the generation of the zonal flow modes (as $\overline{\gamma}_{zf} \approx n_{tr}$ (27)), which represent the second possible influence on the drift turbulence. They action is indirect and consists of the modification of the diffusion and/or of the structures. The third mechanism is provided by the diffusion, which can be strongly changed by the structures.

The results presented in the Figures 6-8 show a strong action of the third mechanism at the beginning of the nonlinear stage, around $t = 3$. Trajectory trapping determines a strong increase of the diffusion coefficient D_2, which drives the turbulence back in the quasilinear regime. The process last for a short time interval, and it is eliminated by the decrease of the wave numbers of the drift turbulence, which reduces strongly the diffusive damping in the growth rate (25). The decrease of the wave numbers is due to the narrowing of the spectrum as the effect of increased diffusion. Thus, a complex transient process of interaction appears at this stage, which is the result of increased diffusion which determines both the increase and the decrease of the diffusive damping. The other two mechanisms determine the evolution at later time when the zonal flow modes reach amplitudes that are comparable to Φ. The zonal flow modes determine the increase of the structures due the the modification of the potential. The fraction of trapped trajectories increases, the structure have larger size and they become elongated in the direction of the zona flow modes. This leads to the decay of the drift turbulence which acquire negative growth rates. The zonal flow effect is produced through the

quasi-coherent structures, rather than through the diffusion in the system studied here.

In conclusion, the results obtained in this paper bring a new image on nonlinear processes associated to the generation of quasi-coherence in particle trajectories. They apply to the drift turbulence in a simple confinement geometry (uniform magnetic field), but we expect that similar processes can be found in more realistic models of turbulence. A semi-analytical method that could be extended to other types of turbulence was developed.

Acknowledgements

This work was supported by the Romanian Ministry of National Education under the contract 1EU-10 that is included the Programme of Complementary Research in Fusion. The views presented here do not necessarily represent those of the European Commission. The last part of this work was supported on the contract PN-16470101.

[1] Provenzale A 1999 *Annu. Rev. Fluid Mech.* 31 55
[2] Krommes J A 2002 *Phys. Reports* 360 1
[3] Falkovich G, Gawedzki K and Vergassola M 2001 *Rev. Mod. Phys.* 73 913
[4] Kraichnan R H and Montgomery D 1980 *Rep. Progr. Phys.* 43 547
[5] Terry P W 2000 *Rev. Mod. Phys.* 72 109
[6] Diamond P H, Hasegawa A and Kima K 2011 *Plasma Phys. Control. Fusion* 53 124001
[7] Diamond P H, Itoh S-I, Itoh K and Hahm T S 2005 *Plasma Phys. Control. Fusion* 47 R35
[8] Kraichnan R H 1970 *Phys. Fluids* 19 22
[9] Balescu R 2005 *Aspects of Anomalous Transport in Plasmas*, Institute of Physics Publishing (IoP), Bristol and Philadelphia
[10] Neuer M, Spatschek K H 2006 *Phys. Rev. E* 74 036401
[11] McComb W D 1990 *The Physics of Fluid Turbulence,* Clarendon, Oxford
[12] Vlad M, Spineanu F, Misguich J H and Balescu R 1998 *Phys.Rev.E* 58 7359
[13] Vlad M and Spineanu F 2004 *Phys. Rev. E* 70 056304
[14] Vlad M 2013 *Phys. Rev. E* 87 053105
[15] Dupree T H 1966 *Phys. Fluids* 9 1773
[16] Dupree T H 1972 *Phys. Fluids* 15 334
[17] Taylor G I 1921 *Proc. London Math. Soc.* 20 196
[18] Bouchaud J-P and Georges A 1990 *Phys. Reports* 195 127
[19] Bassu R, Jessen T, Naulin V and Rasmussen J J 2003 *Phys. Plasmas* 10 2696
[20] Hauff T and Jenko F 2007 *Phys. Plasmas* 14 092301
[21] Corrsin S 1959, in Atmospheric Diffusion and Air Pollution, ed. F. Frenkel & P. Sheppard (Advances in Geophysics, Vol. 6, Academic, New York), 161
[22] Gruzinov A V, Isichenko M B and Kalda Y L 1990 *Sov. Phys.-JETP* 70, 263
[23] Isichenko M B 1991 *Plasma Phys. Control. Fusion* 33 809
[24] Vlad M and Spineanu F 2015 *Phys. Plasmas* 22 112305
[25] Vlad M and Spineanu F 2013 *Phys. Plasmas* 20 122304
[26] Vlad M, Spineanu F, Misguich J H, Reuss J-D, Balescu R, Itoh K and Itoh S-I 2004 *Plasma Phys. Control. Fusion* 46 1051
[27] Vlad M, Spineanu F 2011 *Romanian Journal of Physics* **56** Supplement 23
[28] Neur M and Spatschek K H 2008 *Phys. Plasmas* 15 022304
[29] Petrisor I, Negrea M and Weyssow B 2007 *Physica Scripta* 75 1
[30] Hauff T and Jenko F 2006 *Phys. Plasmas* 13 102309
[31] Vlad M, Spineanu F and Benkadda S 2006 *Phys. Rev. Lett.* 96 085001
[32] Balescu R, Petrisor I and Negrea M 2005 *Plasma Phys. Control. Fusion* 47 2145
[33] Vlad M, Spineanu F and Benkadda S 2008 *Plasma Phys. Control. Fusion* 50 065007

[34] Vlad M and Spineanu F 2014 *Astrophys. J.* 791 56
[35] Vlad M, Spineanu F and Croitoru A M 2015 *Astrophys. J.* 815 11
[36] Vlad M and Spineanu F 2016 *Nuclear Fusion* 56 092003
[37] Goldstone R J and Rutherford P H 1995 *Introduction to Plasma Physics*, Institute of Physics Publishing, Bristol and Philadelphia
[38] Horton W 1999 *Rev. Modern Phys.* 71 735
[39] Garbet X, Idomura Y, Villard L and Watanabe T H 2010 *Nuclear Fusion* 50 043002

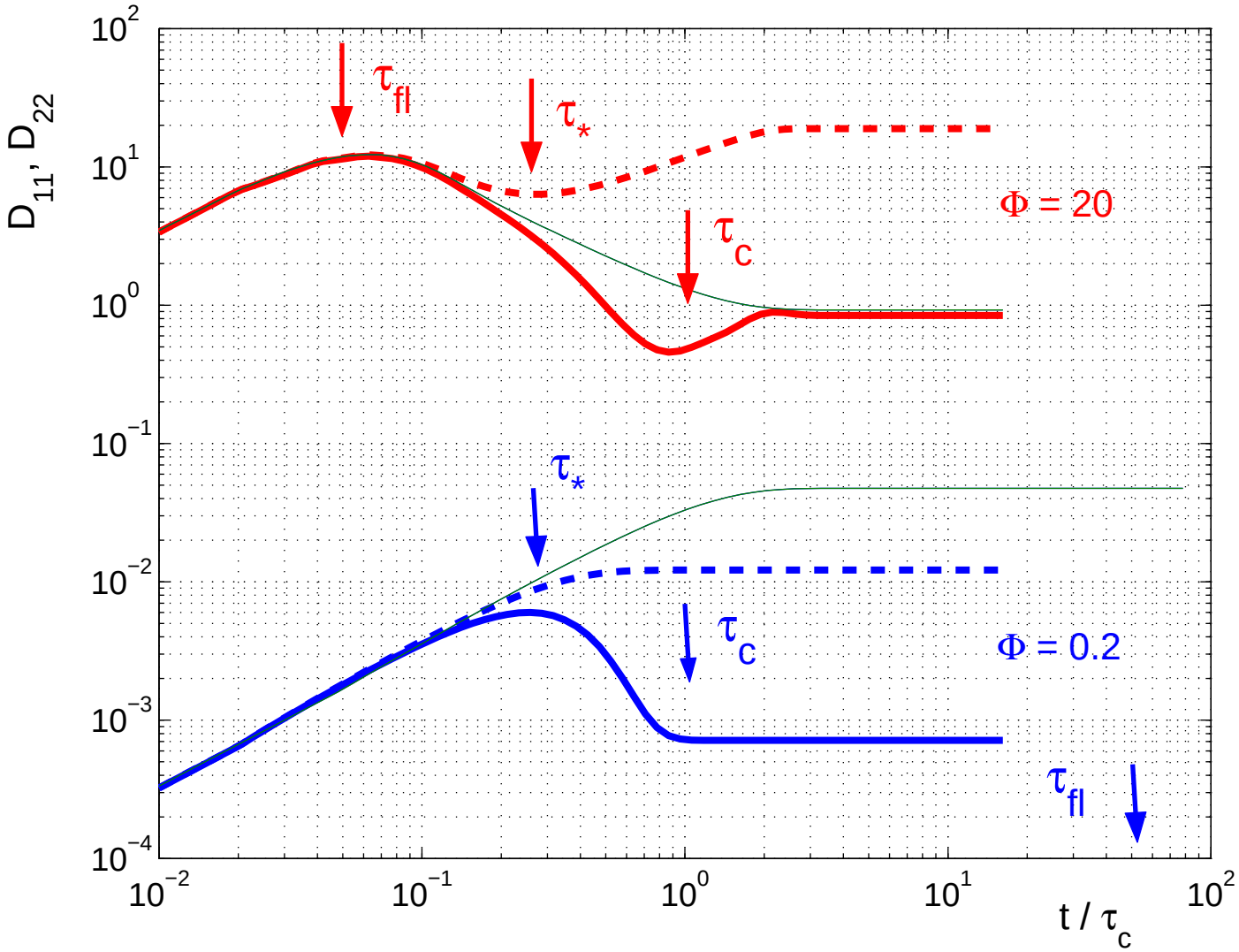
10^2
10^1
10^0
10^{-1}
10^{-2}
10^{-3}
10^{-4}
D_{11}, D_{22}
τ_{fl}
τ_*
τ_c
$\Phi = 20$
τ_*
τ_c
$\Phi = 0.2$
τ_{fl}
10^{-2}
10^{-1}
10^0
10^1
10^2
t / τ_c